33rd Annual International Conference of the IEEE EMBS
Boston, Massachusetts USA, August 30 - September 3, 2011

Comprehensive Mechanism-Based Antibody Pharmacokinetic Modeling

Jeffrey R. Chabot, *Member, IEEE,* Danielle E. Dettling, Paul J. Jasper, and Bruce C. Gomes

Abstract— **Pharmacokinetic models of antibody distribution and dynamics are useful for predicting and optimizing therapeutic behavior. Targeted antigens are produced and distributed in various tissues in specific patterns in disease phenotypes. Existing models leave out significant mechanistic detail which would enable an understanding of how to modify therapeutics in an optimal manner to allow appropriate tissue penetration in either a healthy or diseased state. The model presented here incorporates additional complexity such as diffusion through endothelial barriers, differential transcytosis properties, FcRn-mediated recycling, and incorporates these properties in an organ-specific manner. This creates a platform which can be expanded upon to include understanding of the effect of target on therapeutic distribution and clearance, differences in dynamics during a diseased versus healthy state, differential dose strategies, and mechanistic translation between animal models and human disease state. This model represents a superior alternative to typical and potentially over-simplified scaling strategies utilized in most existing physiologically-based pharmacokinetic models. Ultimately, this will enable better therapeutic design and greater pharmacological effects.**

I. Introduction

MATHEMATICAL models of therapeutic pharmacokinetics and dynamics are generally phenomenological in nature. Biological agents, including antibodies and other large molecule protein therapeutics, represent a special class of pharmaceuticals with some properties largely conserved between agents; for example, clearance by kidney filtration has been shown to depend mostly upon the size of globular proteins [1]. Several mechanistic models of therapeutic antibody distribution and clearance have been generated (for example, [2-3]). These models generally select a few aspects of antibody kinetics (e.g., diffusion through pores, recycling machinery), and fit the parameters associated with these processes to a data set representing a limited number of experimental conditions.

The advantages of a mechanistic model of therapeutic kinetics are manifold. While static measurements may offer a snapshot of the therapeutic exposure of an organ representing the site of action, understanding distribution dynamics can dramatically affect the interpretation of these measurements. For example, an organ with low exposure but rapid turnover may experience a greater therapeutic effect than another organ with greater absolute exposure but slower exchange. A model may help to estimate the therapeutic window between efficacious therapeutic benefit and potential safety liabilities, and to optimize dosing regimens to maintain performance within this window. A mechanistic model may also be systematically adjusted to represent different individual parameters or phenotypes, including disease states which often significantly alter tissue physiology (for example, reduced kidney clearance in individuals with impaired renal function).

While an appropriate model necessarily includes a significant reduction in complexity, the risk of oversimplification combined with parameter estimation from data is that the parameters thus determined actually represent "lumped" behavior from both modeled and unmodeled processes. The resulting model may adequately fit the data used for training, but how these "effective" parameters should be modified under different conditions is unclear (short of actually performing a new experiment, reducing the utility of the model as a predictive tool).

II. Model Description

A. Overview

In this work, we describe a more comprehensive mechanistic model of antibody pharmacokinetics than has previously been generated. This model includes a number of organs, which have been shown to be responsible for 95% of antibody disposition at 1h time [3]. Fluid and soluble components are transmitted between these organs via blood and lymphatic flow. Generally, organs contain several different spaces (compartments), usually representing tissue interstitium and endosomes of endothelial cells. Antibodies are transmitted between these compartments via several processes, including diffusion, capillary and venous convection, and transcytosis. Clearance occurs when the therapeutic is not rescued from lysosomal degradation via an FcRn-mediated process, or via kidney filtration. All processes proceed against a background of endogenous antibody production and clearance.

The model describes IgG, $F(ab')_2$, and Fab' distribution and dynamics in mice. It is constructed using a number of parameters determined from the literature, where such values can be found or extracted from published data. The

Manuscript received 15 April 2011.

J. R. Chabot is employed by Pfizer, Inc., Research Technology Center, Cambridge, MA 02139 USA (phone: 617-551-3279; fax: 617-551-3082; e-mail: jeffrey.chabot2@pfizer.com).

D. E. Dettling is employed by Pfizer, Inc., Rinat Laboratories, San Francisco, CA 94080 USA. (phone: 650.615.7466; e-mail: danielle.dettling@pfizer.com).

P. J. Jasper is employed by RES Group, Inc., Cambridge, MA 02139 USA (email: pjasper@resgroupinc.com).

B. C. Gomes is employed by Pfizer, Inc., Research Technology Center, Cambridge, MA 02139 USA (e-mail: bruce.gomes@pfizer.com).

remaining model parameters are fitted simultaneously to a number of experiments identified in the literature, including:

long-term (several days) plasma concentrations in normal mice [4];

long-term (several days) plasma concentrations in β-2-microglobulin (β2m) knockout mice (lacking functioning FcRn recycling machinery) [4];

short-term (less than one day) organ and plasma concentration data for IgG, $F(ab')_2$, and Fab' [5]; and

plasma clearance rates in hyperimmunized mice (overproducing endogenous IgG, enhancing clearance by oversaturating the FcRn machinery) [6].

B. Top-level model structure

The organs modeled are the lungs, kidneys, liver, spleen, GI, skin, muscle, and heart. Plasma flow between the organs is obtained from [7], scaled as 50% of blood flow to exclude the volume occupied by cells and therefore inaccessible to typical biotherapeutics. Plasma flow to the heart represents the blood supply of the cardiac tissue, not flow through the chambers of the heart. Generally, plasma flows from a general pool (representing the vascular volume not contained in the modeled organs) to the vasculature of the various organs, to the vascular space of the lungs, and back to the general pool. The exceptions to this flow are the spleen and GI, whose blood flows through the hepatic portal vein to the liver, where it mixes with blood coming directly from the general pool.

Lymphatic flow from each organ is assumed proportional to the blood flow Q to that organ. There are two constants of proportionality, one for liver and GI, and another for the remaining tissues. These constants are determined by setting the total lymph flow from liver and GI to be two thirds of the total body lymph production [8], and setting the total lymph production tos 0.004 ml/min [8]. This flow moves from the interstitium of the organs (with no filtration through the open-ended lymphatic network) and rejoins the plasma in the general pool. The vascular plasma outflow from each organ is reduced by this amount to conserve volume in the system.

In each space, the concentrations of the therapeutic and the endogenous IgG are monitored. The two species are otherwise indistinguishable, with the exception that the endogenous IgG is constitutively expressed, while the therapeutic IgG is periodically administered.

The organ connection scheme is depicted in Figure 1(a).

C. Internal organ structure

Within an organ, the vascular, interstitial, and endosomal volumes are obtained from [7] (the vascular volume is reduced by 50% for the same reason as blood flow above); concentrations in these spaces are C_V, C_I, and C_E respectively. Soluble factors transfer between the spaces as follows:

1) Vascular-interstitial exchange: Plasma is assumed to move by convection from capillaries into interstitium through one set of pores (characterized by volume flow rate J_C and reflection coefficient σ_C) and back into veins through another set (J_V, σ_V). The parameter σ_C was allowed to adopt two values, one for GI and liver to reflect the different fenestration of these organs, and another for the remaining organs. The flow rates are calculated based on the lymphatic flow; it has been estimated that lymphatic outflow represents 10% of the volume moving into the interstitium from the capillaries, with the rest returning into the veins. Diffusion also occurs through both capillary pores (with permeability-surface area products PS_C and Peclet ratio Pe_C, defined as

$$Pe_C = \frac{J_C(1-\sigma_C)}{PS_C},$$

and venous pores (PS_V, Pe_V). The net flux from vasculature to interstitium per unit time is given by

$$J_C(1-\sigma_C)C_V + PS_C \cdot (C_V - C_I)\frac{Pe_C}{e^{Pe_C}-1} + J_V(1-\sigma_V)C_I + PS_V \cdot (C_V - C_I)\frac{Pe_V}{e^{Pe_V}-1}.$$

It should be noted that not all fluid transferred between these compartments need be communicated through the pores described; instead the flux should be multiplied by a coefficient of hydraulic conductivity. However, as this coefficient is bounded between zero and unity, the term $(1-\sigma)$ may absorb this coefficient. The interpretation of the

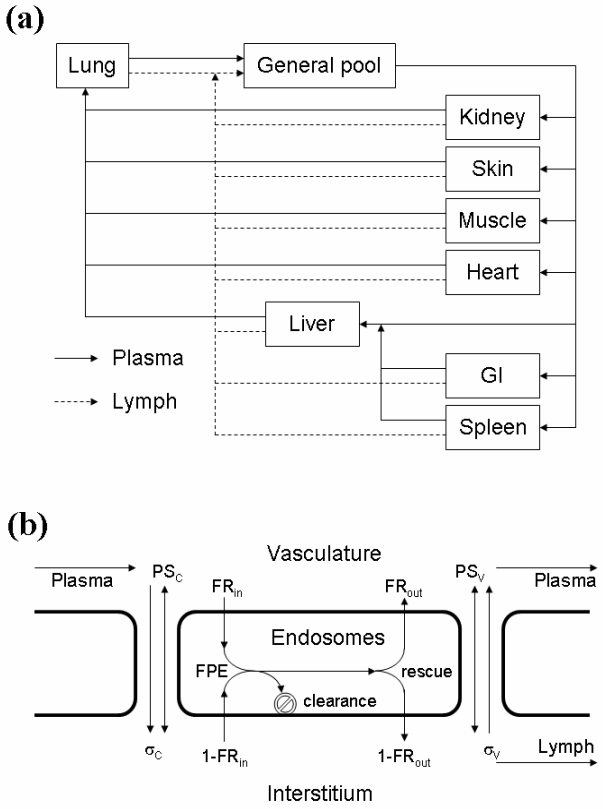

Fig. 1. General model scheme. (a) Connection of organs, including plasma and lymphatic flow. (b) Intra-organ transport processes, including convection (reflection coefficients σ_C, σ_V), diffusion (permeability-surface area products PS_C, PS_V), fluid phase endocytosis uptake (polarized by FR_{in}), rescue or clearance of endocytosed material, and output (polarized by FR_{out}).

values of σ determined using this model should include this consideration.

2) Vascular-endosomal exchange: Plasma is taken up by the endosomes of the endothelium by fluid phase endocytosis (total rate *TotFPErate*, polarized by FR_{in}). The total fluid phase endocytosis rate is determined by dividing the vascular surface area within the organ [9-11] by the cross sectional area of an endothelial cell (estimated at 30 μm by 12 μm) to determine the number of endothelial cells, and multiplying by a rate *FPE_per_cell*. Once material has been taken up, a certain fraction A is automatically "rescued" (otherwise, the whole-body rate of uptake would clear non-recycled material such as Fab's with a much faster rate than is observed). The rest of the material (consisting of endogenous and exogenous antibody) is assumed to be in rapid equilibrium binding with the FcRn receptor with binding affinity K_D. The FcRn concentration [*FcRn*] is determined by multiplying a parameter *FcRn_per_cell* by the number of endothelial cells determined above. The (automatically or FcRn-mediated) rescued material is returned to the plasma with the same bulk flow rate *TotFPErate* and polarization FR_{out}, for a net vascular-to-endosomal amount transfer rate of

$$TotFPErate \cdot FR_{in} \cdot C_V - TotFPErate \cdot FR_{out}\left(A + \frac{R}{C_{E,tot}}\right)C_E$$

where $C_{E,tot}$ represents the sum of endogenous and exogenous IgG in the endosomes, and R (the recycled fraction) is defined by

$$K_D + [FcRn] + (1-A)C_{E,tot} - 0.5\{(K_D + [FcRn] + (1-A)C_{E,tot})^2 - 4(1-A)C_{E,tot}[FcRn]\}^{0.5}$$

3) Interstitial-endosomal exchange: Exchange between interstitium and endosomes is similar to vascular-endosomal exchange, with polarizations (1-FR_{in}) for uptake and (1-FR_{out}) for return, for a net amount transfer from interstitium to endosomes of

$$TotFPErate \cdot (1-FR_{in})C_V - TotFPErate \cdot (1-FR_{out})\left(A + \frac{R}{C_{E,tot}}\right)C_E$$

with R defined as above.

4) Lymphatic clearance: Given a lymphatic flow rate coefficient L determined as previously described for a given organ, the amount of material in the interstitium of an organ is further reduced by the rate

$$Q \cdot L \cdot C_I ,$$

with the removed material transferred to the general plasma pool.

5) Endosomal clearance: The amount of material not rescued from the endosomes is irreversibly moved into a pool contained within the endosomal space (representing, for example, lysosomes); however, any radiolabel will continue to provide signal in an experiment. Therefore, this pool is included when calculating total signal from an organ. The amount in this pool is subject to first-order decay with a 24 hour time scale.

The processes transfer between organ components are summarized in Figure 1(b).

D. Special organs

The following organs are treated differently based on physiology:

1) Kidney: The kidney effectively has no interstitium, as the glomerular basement membrane effectively prevents macromolecules from crossing into a true "interstitial" space. Endosomal mechanics are also excluded in this organ. We do, however, include kidney filtration of soluble species. A volume equal to the glomerular filtration rate (*GFR*) is moved into a separate "nephron" compartment; the fraction of a given species X contained in this volume which is transported is defined to be θ_X, the glomerular sieving coefficient. The contents of this nephron compartment are either reabsorbed to the plasma (fraction B) or cleared to the urine (and removed from the system, fraction 1-B), with a time scale defined by the mean transit time (*MTT*).

2) Spleen: The spleen has no interstitial or endosomal space, as the vasculature effectively "disappears" within the red pulp region to allow for efficient clearance of old red blood cells. The vascular space is increased by 22% to account for this additional volume (calculated from [12]).

3) Liver: The vascular volume of the liver includes not only half of the vascular volume from [7], but also the full volume of the Space of Disse [13], as the sinusoidal membrane separating this space from the true vascular space excludes cells but allows macromolecules to freely mix throughout this region. The endothelial cells lining this space (twice as many as for the rest of the liver, based on [13]) effectively "face" the vascular space on both sides, and therefore the fluid phase endocytosis uptake and return do not include polarization terms (but do still include the recycling machinery). Additionally, the permeability-surface area products PS_C and PS_V are increased by a factor of ten (an assumption from [3]).

4) Other endosomes: We include an additional "tissue" representing the endosomes of endothelial cells not contained in the modeled organs. These cells do not interact with any "interstitial" space, but instead use the polarization FR_{in} for both uptake from and return to the vascular space.

III. Model Implementation

The parameters involved in the model are listed in Table 1. The values are obtained directly or derived from the literature, estimated based on prior experience, or fitted to the experiments described above. The data from these experiments were determined by digitization of the figures from the papers and extraction of numerical values using MATLAB.

The model was written, analyzed, and calibrated in OpenBio Pro (RES Group Inc., openbio.resgroupsoftware.com), a powerful and efficient

TABLE I
MODEL PARAMETERS

Symbol	Quantity	Value/Range[a]	Source
V_v, V_i, V_e	Vascular, interstitial, endosomal volumes	various	[7][b]
Q	Plasma flow to organ	various	[7][b]
$L_{GI,Liver}$	Lymphatic flow coefficient from GI, liver	0.00081	[8] (derived)
L_{other}	Lymphatic flow coefficient for other organs	0.00024	[8] (derived)
K_D	IgG-FcRn affinity	750 nM	[14]
GFR	Glomerular filtration rate	0.1 mL / min	[15]
MTT	Mean nephron transit time	4 min	[16-18][c]
B	Nephron-to-plasma protein reabsorption coefficient	0.927 (dimensionless)	[7,14] (derived)
A	Automatic recycling faction	1e-4 – 1 (dimensionless)	Fitted
FPE_per_cell	Fluid phase endocytosis rate per cell	2.7e-4 – 2.7 pL/hr	Fitted
$FcRn\_per\_cell$	FcRn receptors per cell[d]	1e3 – 1e7 (dimensionless)	Fitted
σ_C	Capillary reflection coefficient[e]	1e-4 – 1 (dimensionless)	Fitted
$\sigma_{C,Liver/GI}$	Capillary reflection coefficient in liver and GI[e]	1e-4 – 1 (dimensionless)	Fitted
σ_V	Venous reflection coefficient[e]	1e-4 – 1 (dimensionless)	Fitted
θ	Glomerular sieving coefficient[e]	1e-4 – 1 (dimensionless)	Fitted
FR_{in}	Polarization of FPE uptake	1e-4 – 1 (dimensionless)	Fitted
FR_{out}	Polarization of FPE output	1e-4 – 1 (dimensionless)	Fitted
PS_C	Permeability-surface area product (capillary)[f]	1.6e-5 – 1.6e-3 mL hr^{-1} g^{-1}	Fitted
PS_V	Permeability-surface area product (vein)[f]	4.7e-5 – 4.7e-3 mL hr^{-1} g^{-1}	Fitted

[a]Values for fixed parameters ; ranges for fitted parameters.
[b]Vascular volumes and blood flow rates are divided by two to correct blood volumes and flows to plasma volumes and flows.
[c]Typical mammalian value; human ~4-5 min [16], rat 1-7 min [17,18]
[d]Converted to a concentration using 1 pL volume per cell and 20% of this volume as the endosomal volume.
[e]Different values for IgG, $F(ab')_2$, and Fab', constrained as described in text.
[f]Values in specific organs scaled by organ mass, taken as total organ volume multiplied by 1.05 g/mL.

ODE simulator with integrated sensitivity analysis and parameter estimation features. All parameters were simultaneously estimated, fitting to all experiments using a parameter estimation algorithm with a normalized weighted least squares objective function. To recapture the appropriate experimental conditions, the simulations used for fitting experiments were modified in the following way:

1) Long-term plasma data in normal mice: No change.

2) Long-term plasma data in β2m knockout mice: *FcRn_per_cell* set to zero.

3) Organ data (IgG): No change.

4) Organ data ($F(ab')_2$): *FcRn_per_cell* set to zero; PS_C, PS_V increased by a factor of three.

5) Organ data (Fab'): *FcRn_per_cell* set to zero; PS_C, PS_V increased by a factor of twenty.

6) Hyperimmunized mice: Endogenous synthesis rate set to give total plasma level of endogenous IgG measured in each experimental group (mice were clustered by plasma IgG concentration, correlating inversely with measured half life). The therapeutic half life was defined by

$$t_{1/2} = \frac{\ln(2) \cdot C_{plasma}}{\dot{C}_{plasma}}$$

with $\dot{C}_{plasma}$ representing the rate of change of therapeutic concentration in plasma, and was fit to the observed half life at days 4, 6, 9, and 12 with increasing weight on each time.

A further constraint was introduced that all reflection coefficients strictly increased and glomerular filtration coefficients strictly decreased with molecular size ($\sigma_{Fab'} < \sigma_{F(ab')2} < \sigma_{IgG}$, $\theta_{Fab} > \theta_{F(ab')2} > \theta_{IgG}$). In all, 162 data points and 8 constraints were used in fitting the 19 parameters in Table 1.

IV. RESULTS

To begin model calibration, starting parameter values were randomly selected from within the ranges listed for the fitted parameters in Table 1. For parameters with a logarithmic scale (e.g., *FPE_per_cell*), values were randomly selected using a logarithmic range; others with a linear scale (e.g., FR_{in}) were randomly selected from a linear range. Five thousand independent parameter estimations were performed using Pfizer's high-performance computing cluster. The 1% of parameter sets giving the lowest final objective functions were selected for analysis. The fits obtained from the single best-fitting solution are shown in Figure 2. The average parameter values in these fifty best solutions are given in Table 2; parameters distributed ranging on a log scale are represented by their logarithmic average.

The model recaptures the salient features of each data set, including (for example) the delayed peak in exposure of the GI compared to other organs; the relative exposures and time scales of the different molecules simulated (IgG., $F(ab')_2$, Fab'); the effect of knocking out the FcRn recycling machinery on IgG clearance; and the decreasing trend in antibody half life with increasing endogenous antibody production. The model output corresponding to the long-term plasma time course data in wild-type animals (Figure 2(b)) is consistently lower. However, the major information content in this data is the half life, which the model approximates well (nearly parallel trajectories); the model also recaptures the change in clearance rate upon elimination of the FcRn machinery.

To estimate the relative importance of each parameter, the fraction of parameter space occupied by the best solutions was computed, represented by the fraction of total space occupied by two standard deviations of the parameter values from this set, log transformed if appropriate. Since the initial distribution of parameter values is uniform across these ranges, if the model did not select a particular value, we would expect this range to be approximately 58% of the range. However, for nearly all parameters, the actual "good-solution" space is less than ten percent of the possible range, suggesting that these parameters play an important role in the performance of the model with respect to the fitted

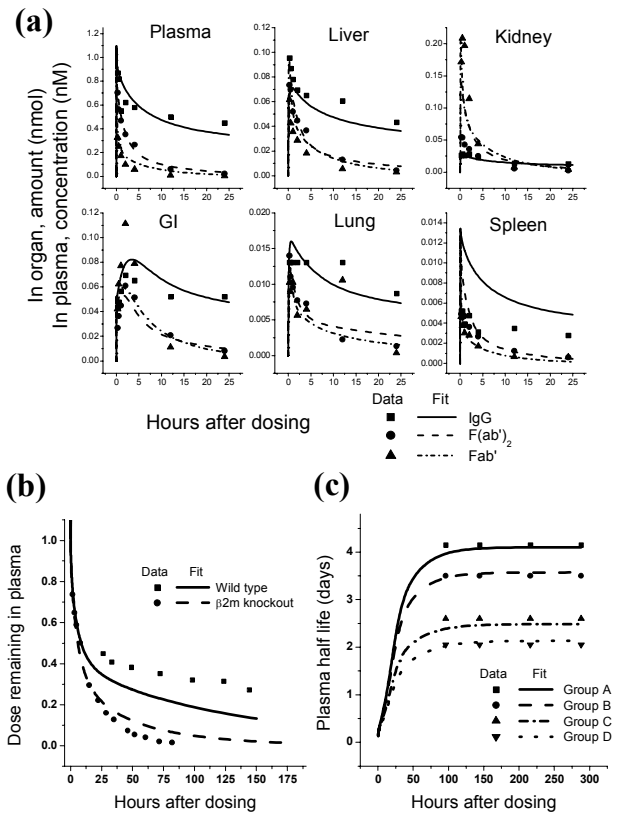

Fig. 2. Comparison of model with optimized parameters versus training data. (a) Organ fit data for IgG, $F(ab')_2$, Fab' (data from [5]). (b) Plasma fit for IgG in normal or β2m knockout animals (data from [4]). (c) IgG half life for hyperimmunized mice (grouped by circulating endogenous IgG level, A<B<C<D; data from [6]).

experiments, and perhaps placing a range on the actual parameter values found in across population of similarly-behaving individuals.

V. Discussion

The model as presented and parameterized may be useful in its current form to gain further insight than is evident in the data used for informing it. For example, the dynamic rate of turnover in a given organ, the division of the dose between organ compartments (vascular, endosomal, interstitial), or the amount of signal coming from intact versus cleared therapeutic may be estimated. Potentially, however, the greatest utility of this model as a predictive tool comes from the expansion or translation of the model onto different experimental systems. Such modifications may include:

1) Inclusion of additional organs, such as tumor (for cancer applications), adipose (diabetes and/or obesity), cartilage and synovial fluid (osteo- or rheumatoid arthritis), bone (osteoporosis, multiple myeloma) or brain/central nervous system (Alzheimer's disease, other neurological disorders).

2) Currently included organs may be expanded to include aspects particular to specific disease states. For example, lung compartments may be represented more specifically for respiratory disorders (e.g., viral/bacterial infection, allergies).

3) Alternative dosing schemes; for example, subcutaneous administration by introducing dose into the adipose compartment mentioned above, intracranial or intrathecal injection, etc.

4) Introduction of therapeutic binding to a target (soluble or membrane-bound) differentially expressed between the various organs to estimate neutralization of target and pharmacological effect.

5) Translation of parameters (e.g., organ size, blood and lymph flow rates) to a different species (e.g., monkey, human) to anticipate pharmacokinetic and/or pharmacodynamic properties and how such properties may change from a preclinical to clinical setting.

6) Modification of parameters or processes to reflect different phenotypes representing disease or patient variability (e.g., reduced liver permeability in cases of fibrosis).

7) Introduction of alternative large-molecule therapeutics such as pegylated molecules or peptides, or molecules with altered FcRn binding, multi-antigen specific therapeutic modalities, antibody-drug conjugates, etc.

As antibody and other large biomolecule based therapies become increasingly utilized for oncological, inflammatory, autoimmunological, and other conditions, it will become necessary to better understand and manipulate therapeutic properties. Further, the ability to anticipate pharmacokinetic and pharmacodynamic behaviors and to optimize the relevant properties of a proposed therapeutic in a preclinical discovery setting may substantially increase the success rate of research efforts. The use of mechanistic, predictive models of biotherapeutic pharmacokinetics will be an essential tool for the continued development of this important class of pharmaceutical agents.

TABLE II
Fitted Parameter Values

Symbol	Optimized value	Fraction of range occupied by +/- 1 S.D.
A	0.0564	8.9%
FPE_per_cell[a]	0.0117	4.6%
$FcRn\_per\_cell$[a]	6.9e5	2.5%
$\sigma_{C,IgG}$	0.897	3.3%
$\sigma_{C,F(ab')2}$	0.871	4.0%
$\sigma_{C,Fab'}$	0.578	17.2%
$\sigma_{C,IgG,Liver/GI}$	0.906	2.4%
$\sigma_{C,F(ab')2,Liver/GI}$	0.848	6.5%
$\sigma_{C,Fab',Liver/GI}$	0.595	17.0%
$\sigma_{V,IgG}$	0.202	24.1%
$\sigma_{V,F(ab')2}$	0.0518	8.6%
$\sigma_{V,Fab'}$	0.0174	3.3%
θ_{IgG}	0.02614	0.37%
$\theta_{F(ab')2}$	0.403	10.3%
$\theta_{Fab'}$	0.990	0.66%
FR_{in}	0.971	14.7%
FR_{out}	0.364	40.4%
PS_C[a]	1.4e-4	66.8%
PS_V[a]	4.7e-3	19.3%

Parameter units as in Table I.
[a]Log of parameter value used for averaging and determining percentage of range spanned by +/- 1 standard deviation.

ACKNOWLEDGMENT

We acknowledge the support of the members of the Biotherapeutics Modeling Team at Pfizer, Inc., specifically, Natalia Boukharov, Matthew Crawford, Kapil Mayawala, Jerome Mettetal, Ling Li, Madhusudan Natarajan, and Weifan Weng. We further acknowledge model implementation assistance from John Tolsma and Brian Simpson of RES Group, Inc.

REFERENCES

[1] D. Venturoli and B. Rippe, "Ficoll and dextran vs. globular proteins as probes for testing glomerular permselectivity: effects of molecular size, shape, charge, and deformability," *Am J Physiol Renal Physiol,* vol. 288, pp. F605-13, Apr 2005.

[2] A. Garg and J. P. Balthasar, "Physiologically-based pharmacokinetic (PBPK) model to predict IgG tissue kinetics in wild-type and FcRn-knockout mice," *J Pharmacokinet Pharmacodyn,* vol. 34, pp. 687-709, Oct 2007.

[3] J. P. Davda, M. Jain, S. K. Batra, P. R. Gwilt, and D. H. Robinson, "A physiologically based pharmacokinetic (PBPK) model to characterize and predict the disposition of monoclonal antibody CC49 and its single chain Fv constructs," *Int Immunopharmacol,* vol. 8, pp. 401-13, Mar 2008.

[4] R. P. Junghans and C. L. Anderson, "The protection receptor for IgG catabolism is the beta2-microglobulin-containing neonatal intestinal transport receptor," *Proc Natl Acad Sci U S A,* vol. 93, pp. 5512-6, May 28 1996.

[5] O. D. Holton, 3rd, C. D. Black, R. J. Parker, D. G. Covell, J. Barbet, S. M. Sieber, M. J. Talley, and J. N. Weinstein, "Biodistribution of monoclonal IgG1, F(ab')2, and Fab' in mice after intravenous injection. Comparison between anti-B cell (anti-Lyb8.2) and irrelevant (MOPC-21) antibodies," *J Immunol,* vol. 139, pp. 3041-9, Nov 1 1987.

[6] J. L. Fahey and A. G. Robinson, "Factors Controlling Serum Gamma-Globulin Concentration," *J Exp Med,* vol. 118, pp. 845-68, Nov 1 1963.

[7] B. Davies and T. Morris, "Physiological parameters in laboratory animals and humans," *Pharm Res,* vol. 10, pp. 1093-5, Jul 1993.

[8] A. C. Guyton and J. E. Hall, *Human physiology and mechanisms of disease*, 6 ed.: Saunders, 1996.

[9] J. B. Bassingthwaighte, "A concurrent flow model for extraction during transcapillary passage," *Circ Res,* vol. 35, pp. 483-503, Sep 1974.

[10] C. Crone and D. G. Levitt, "Capillary permeability to small solutes.," in *The Microcirculation, Handbook of Physiology* E. M. Renkin and C. C. Michel, Eds. Bethesda: American Physiological Society, 1984, pp. 411-466.

[11] M. J. Eppihimer, J. Russell, R. Langley, G. Vallien, D. C. Anderson, and D. N. Granger, "Differential expression of platelet-endothelial cell adhesion molecule-1 (PECAM-1) in murine tissues," *Microcirculation,* vol. 5, pp. 179-88, 1998.

[12] I. C. MacDonald, E. E. Schmidt, and A. C. Groom, "The high splenic hematocrit: a rheological consequence of red cell flow through the reticular meshwork," *Microvasc Res,* vol. 42, pp. 60-76, Jul 1991.

[13] A. Blouin, R. P. Bolender, and E. R. Weibel, "Distribution of organelles and membranes between hepatocytes and nonhepatocytes in the rat liver parenchyma. A stereological study," *J Cell Biol,* vol. 72, pp. 441-55, Feb 1977.

[14] J. Zhou, J. E. Johnson, V. Ghetie, R. J. Ober, and E. S. Ward, "Generation of mutated variants of the human form of the MHC class I-related receptor, FcRn, with increased affinity for mouse immunoglobulin G," *J Mol Biol*, vol. 332, pp. 901-13, Sep 26 2003.

[15] Z. Qi, I. Whitt, A. Mehta, J. Jin, M. Zhao, R. C. Harris, A. B. Fogo, and M. D. Breyer, "Serial determination of glomerular filtration rate in conscious mice using FITC-inulin clearance," *Am J Physiol Renal Physiol*, vol. 286, pp F590-6, Mar 2004.

[16] S. Mizuiri, I. Hayashi, M. Takano, R. Ban, T. Ohara, Y. Sasaki, and A. Hasegawa, "Fractional mean transit time in transplanted kidneys studied by technetium-99m-DTPA: comparison of clinical and biopsy findings," *J Nucl Med*, vol. 35, pp. 84-9, Jan 1994.

[17] A. Zarzuelo, A. Sanchez-Navarro, F. G. Lopez, and J. M. Lanao, "Influence of dose on the disposition kinetics of netilmicin in the isolated kidney of the rat," *Eur J Drug Metab Pharmacokinet*, vol. 27, pp. 127-33, Apr-Jun 2002.

[18] K. Kim, S. H. Kim, C. W. Yang, C. Li, Y. A. Cheung, S. Y. Lee, H. S. Sohn, and S. K. Chung, "Differentiation between acute cyclosporine nephrotoxicity and acute tubular necrosis using enalaprilat renal scintigraphy in rats," *Invest Radiol*, vol. 38, pp. 473-81, Aug 2003.